Supporting Information

Fluorinated-oligomeric Ionic Liquids for High-performance Wide-temperature Solid Zinc Batteries

Ze Chen,[1] Tong Liu,[2] Zhiquan Wei,[3] Yiqiao Wang,[3] Ao Chen,[3] Zhaodong Huang,[3] Duanyun Cao,[*2] Nan Li,[*3] Chunyi Zhi[*3, 4, 5]

[1] School of Interdisciplinary Studies, Lingnan University, 8 Castle Peak Road, Tuen Mun, Hong Kong, China

[2] Beijing Key Laboratory of Environmental Science and Engineering, School of Materials Science and Engineering, Beijing Institute of Technology, Beijing 100081, China.

[3] Department of Materials Science and Engineering, City University of Hong Kong, 83 Tat Chee Avenue, Kowloon, Hong Kong 999077, China.

[4] Hong Kong Center for Cerebro-Cardiovascular Health Engineering (COCHE), Shatin, NT, HKSAR, China.

[5] Hong Kong Institute for Clean Energy, City University of Hong Kong, Kowloon 999077, Hong Kong.

E-mail: dycao@bit.edu.cn; nanli75@cityu.edu.hk; cy.zhi@cityu.edu.hk

Experimental Section

Materials: 1-ethylimidzole ($C_5H_8N_2$), 1,1,1,2,2-pentafluoro-4-iodobutane ($CF_3CF_2(CH_2)_2I$), 1-iodo-1H,1H,2H,2H-perfluorodecane ($CF_3(CF_2)_7(CF_2)_2I$), toluene (Tol), ethylacetate (EtOAc), 1-ethyl-3-methylimidazolium bis(trifluoromethylsulfonyl)imide (EMIMTFSI), zinc bis(trifluoromethanesulfonyl)imide ($Zn(TFSI)_2$), magnesium sulfate ($MgSO_4$), basic aluminum oxide, chloranil (Cl4Q), and dimethyl sulfoxide-d6 ($(CD_3)_2SO$) were purchased from Aladdin. Poly(vinylidene fluoride-co-hexafluoropropylene) (PVHF, average Mw ~400,000) was purchased from Sigma Aldrich.

Synthesis of 1-ethyl-3-1,1,1,2,2-pentafluoro-4-iodobutylimidazolium bis(trifluoromethylsulfonyl)imide (MIMTFSI-4): The synthesis (see the route in Figure S1) and purification of imidazolium salts containing perfluoroalkyl substituents were modified from literatures.[1] First, 40 mmol nonafluorobutyl iodide was dissolved in 40 mL toluene. Subsequently, 45 mmol 1-methylimidzole was added to the solution, and the mixture was refluxed at 90 ^oC under an argon atmosphere for three days. Afterward, a separate liquid phase formed on the bottom of the flask. Upon cooling to room temperature, the remaining solvent was removed through decantation and vacuum drying at 50 ^oC. Fresh toluene was introduced, and the mixture was refluxed for 30 min, followed by solvent removal in vacuo. This purification process was repeated three more times to obtain 1-perfluorobutyl-3-methylimidazolium iodide, which appeared as a viscous, brown liquid. Furthermore, the crude product was dissolved in 100 mL of deionized water at 65 ^oC. $Zn(TFSI)_2$ (30 mmol) was added to the solution, and the mixture was stirred for 3 h. The resulting product was then extracted with 200 mL EtOAc and washed with 150 mL deionized water four times. To confirm the depletion of iodide anions, $AgNO_3$ was added to the separated water phase after the fourth

washing step. The organic phase was dried using $MgSO_4$, and activated carbon was introduced to remove any colored impurities. The mixture was subsequently filtered through a plug of basic aluminum oxide. The filtrate was reduced by rotary evaporation and further dried under vacuum at 55 ^oC overnight to produce a clear, colorless oil.

Synthesis of 1-ethyl-3-1H,1H,2H,2H-perfluorodecylimidazolium bis(trifluoromethylsulfonyl)imide (MIMTFSI-10): The synthesis process for MIMTFSI-10 closely resembled the synthesis method for MIMTFSI-4, except that the raw material was substituted with heneicosafluorodecyl iodide. The resulting product, 1-perfluorodecyl-3-methylimidazolium iodine, appeared as a brown solid. Furthermore, the conversion of the iodide salts to MIMTFSI-10 followed the same synthesis method employed for MIMTFSI-4. The final product obtained was a clear, colorless, viscous oil.

Fabrication of solid polymer electrolytes with ILs-based plasticizers: First, three ILs-based plasticizers were prepared by dissolving $Zn(TFSI)_2$ into EMIMTFSI, MIMTFSI-4, and MIMTFSI-10, respectively, with a molar ratio 1 : 1. Then, PVHF and $Zn(TFSI)_2$ were mixed with a weight ratio of 10 : 0.5 and the mixture was subsequently dissolved in DMF. The IL-based plasticizers were then added to the solution. The suspension was stirred in the sealed flask at 65 ^oC for 3 h, sonicated for 10 min, and then cast onto a glass plate for solvent evaporation at room temperature. Afterward, membranes were obtained through additional drying steps: heating at 70 ℃ for three days under a vacuum and then heating at 110 ^oC for 4 h under a vacuum. Different contents of $Zn(TFSI)_2$/MIMTFSI-10 plasticizers were introduced into the system, denoted as SPE-X, where X represented the weight ratio of $Zn(TFSI)_2$/MIMTFSI-10 plasticizers to the polymer matrix

composed of PVHF and $Zn(TFSI)_2$, ranging from 0 % to 20 %. The SPE-0% represents the control sample of the SPE without IL plasticizer.

Characterization methods: Fourier-transform infrared (FT-IR) spectra were acquired using the PerkinElmer Spectrum II. The ^{1}H-NMR and ^{19}F-NMR spectra were recorded by Avance-400Hz (Bruker) with DMSO-d6 as the solvent and tetramethyl silane (TMS) as the internal standard. Differential scanning calorimetry (DSC) experiments were conducted using a DSC Q2000 (TA Instruments) equipped with Tzero pans. Thermogravimetric Analysis (TGA) was performed using TG/DTA 6300 to determine the polymer content in the composite. Morphology investigations of the products were carried out using a field-emission scanning electron microscope (SEM, FEI Quanta 450 FEG). Raman spectra were recorded with a WITec alpha300 access with a 532 nm laser.

Electrochemical measurements: The ionic conductivity was measured using a stainless steel (SS)||SS coin cell configuration. The SPE was sandwiched between two stainless steel blocking electrodes. Temperature scans of the ionic conductivity of the SPEs were conducted using an oven, with an increment of 15 ^{o}C. A 10 mV AC perturbation and a frequency range of 1 MHz to 0.01 Hz were used for each measurement. The ionic conductivity (σ) was calculated assuming:

$$\sigma=L/(A*R)$$

where L and A represent the thickness and surface area of the solid electrolyte, respectively.

The impedance of the Zn||Zn symmetric cell was measured both before and after polarization with a DC voltage pulse (25 mV) using a Gamry Interface 1000 Potentiostat. The Zn^{2+} ion transference number, t_{Zn}^{2+}, was calculated assuming:

$$t_{zn^{2+}} = \frac{I_{ss}}{I_0} \times \frac{\Delta V - I_0 R_0}{\Delta V - I_{ss} R_{ss}}$$

where I_{ss} and I_0 are the steady-state and initial currents, respectively, and R_{ss} and R_0 are the corresponding steady-state and initial resistances.

Linear sweep voltammetry (LSV) measurements were performed at room temperature using CHI 760D equipment. The reference electrode was Zn metal, and the working electrode was SS. A linear sweep was conducted from -0.3 V to 3 V at a scan rate of 1 mV s^{-1}.

Both coin-2032 and pouch cells were assembled for electrochemical measurements. The coin cell consisted of a Zn foil (with a thickness of 0.1 mm) as the anode electrode, Cl_4Q on carbon clothes (with a loading mass of 3.0 mg cm^{-2}) as the cathode (Cl4Q : carbon black : PVDF = 6:3:1), and the prepared SPEs as the solid electrolyte. The pouch cell utilized Zn foil (with a thickness of 0.1 mm) as the anode and Cl4Q (with a loading mass of 14 mg cm^{-2}) as the cathode. The batteries' cyclic performance and electrochemical properties were characterized using the LAND CT2001A device and CHI 760D electrochemical workstation at various temperatures.

Computational calculation: The molecule dynamics (MD) simulations were performed using a large-scale atomic/molecular parallel simulator (LAMMPS) package.[2] The Amber-formed force field of the polymer was generated by AmberTool.[3] The atomic charge of the ILs was determined by fitting the Restrained Electrostatic Potential (RESP)[4] on the level of HF/6-31G* in Guassian09.[5] The system maintained at 300 K for 5 ns to reach equilibrium. Finally, another 5 ns production run was performed to collect molecular trajectories, with snapshots saved every 5 ps. The system was kept in the isothermal-isobaric ensemble (NPT) for all simulations. The mean square displacement of individual atoms was calculated by the Einstein equation:

$$MSD \equiv \sum_{i}^{N} \left\langle (R_i(t) - R_0(t))^2 \right\rangle$$

where R represents atomic coordinates, N is the total number of atoms, and t denotes the time. The diffusion constant (D) was determined as the slope of MSD versus times, with a factor of 1/6 applied:

$$D = \frac{MSD}{6t}$$

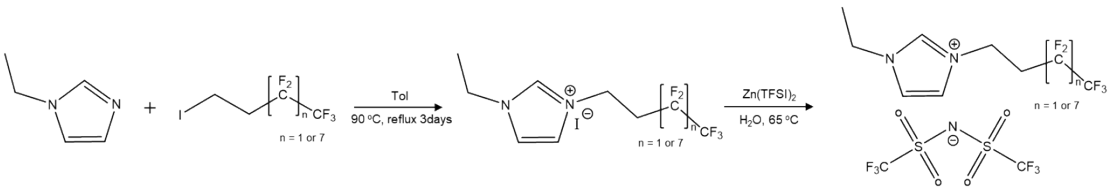

Figure S1. The synthesis route for MIMTFSI-4 and MIMTFSI-10.

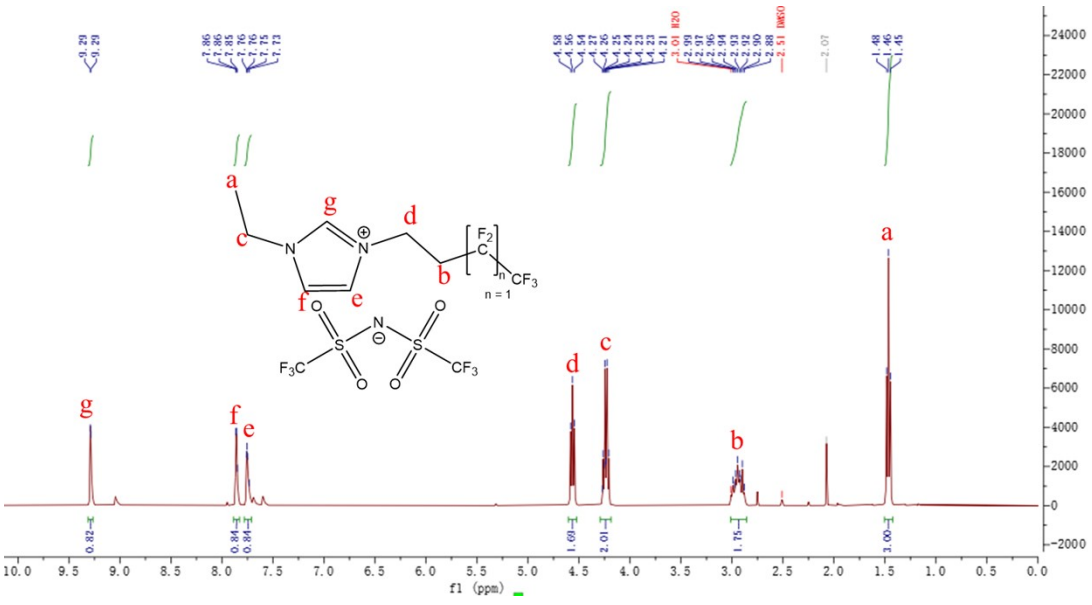

Figure S2. ^{1}H-NMR spectrum of MIMTFSI-4.

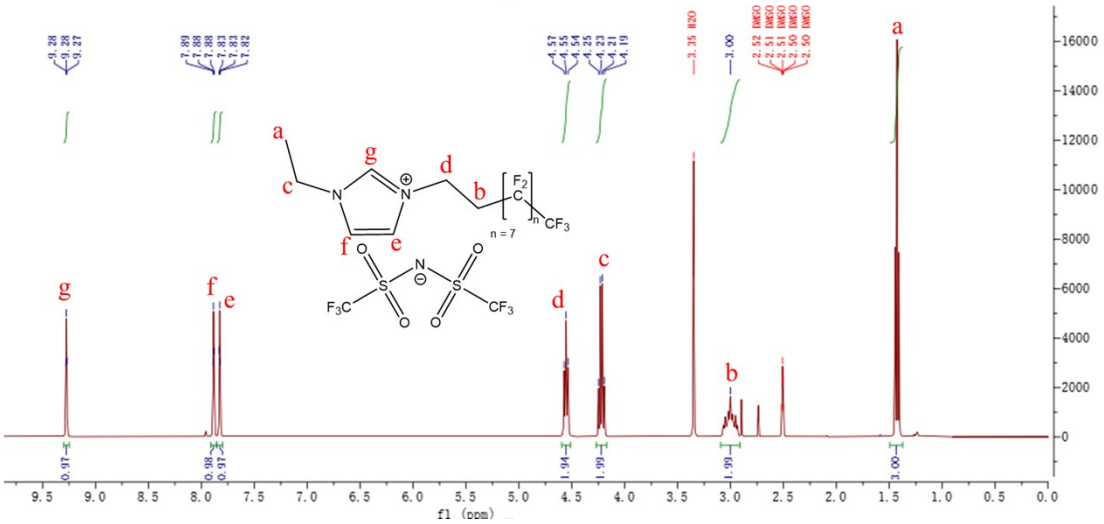

Figure S3. ^{1}H-NMR spectrum of MIMTFSI-10.

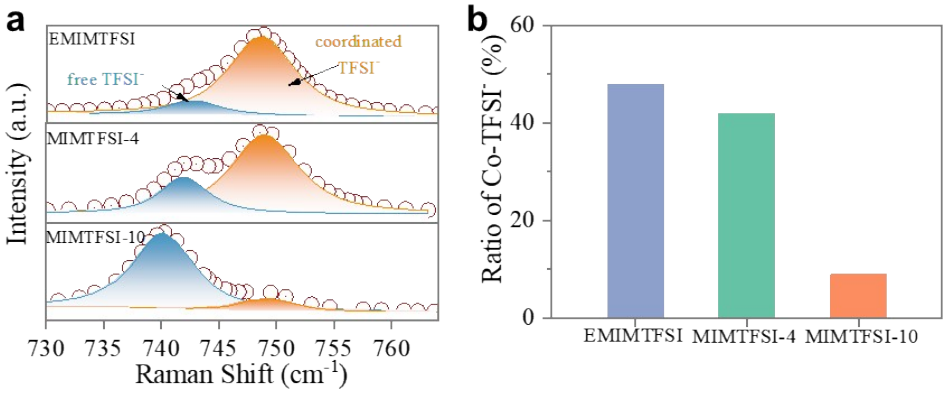

Figure S4. a) Raman spectra of the $Zn(TFSI)_2$/ILs electrolytes and b) the ratio of coordinated $TFSI^-$ ions in $Zn(TFSI)_2$/ILs electrolytes calculated from Raman spectra.

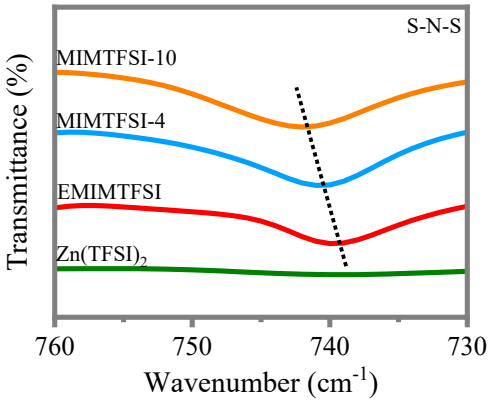

Figure S5. FT-IR spectra of pure $Zn(TFSI)_2$ and 1 M $Zn(TFSI)_2$ in the three ILs.

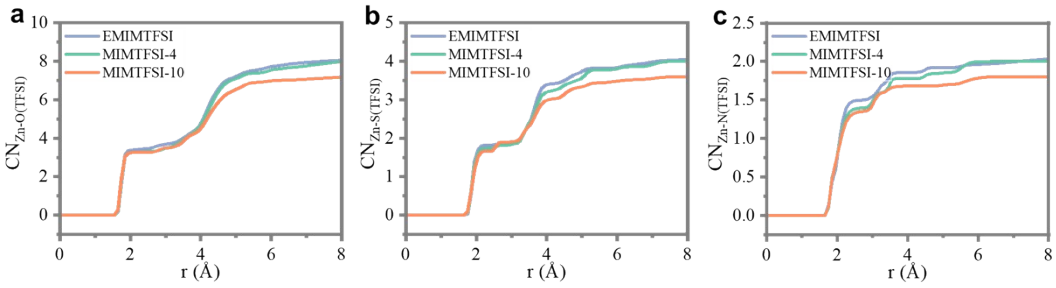

Figure S6. RDF of Zn^{2+} in $Zn(TFSI)_2$/ILs.

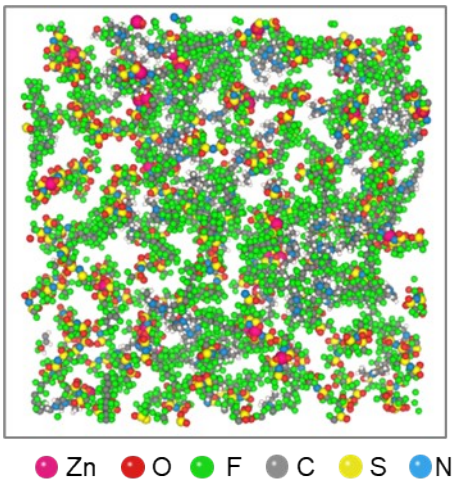

Figure S7. g) snapshot of various solvation structures in $Zn(TFSI)_2$/MIMTFSI-10.

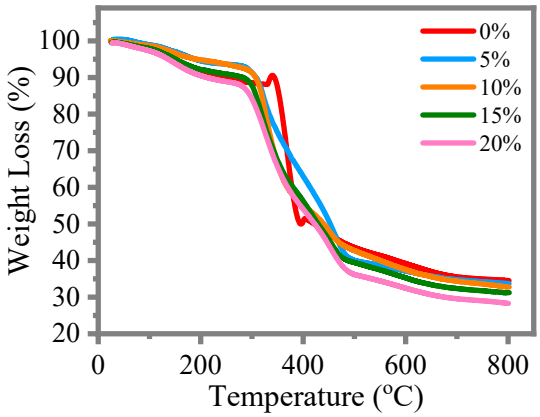

Figure S8. TGA curves of the SPEs with different contents of MIMTFSI-10-based plasticizers.

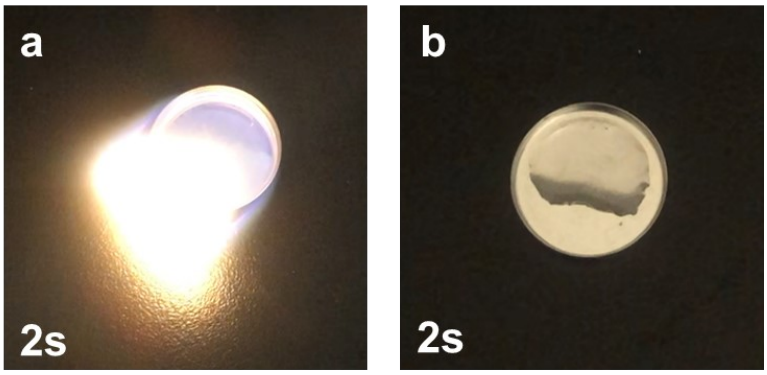

Figure S9. Pictures of the flame test on a) organic electrolytes and b) MIMTFSI-10-based IL electrolytes.

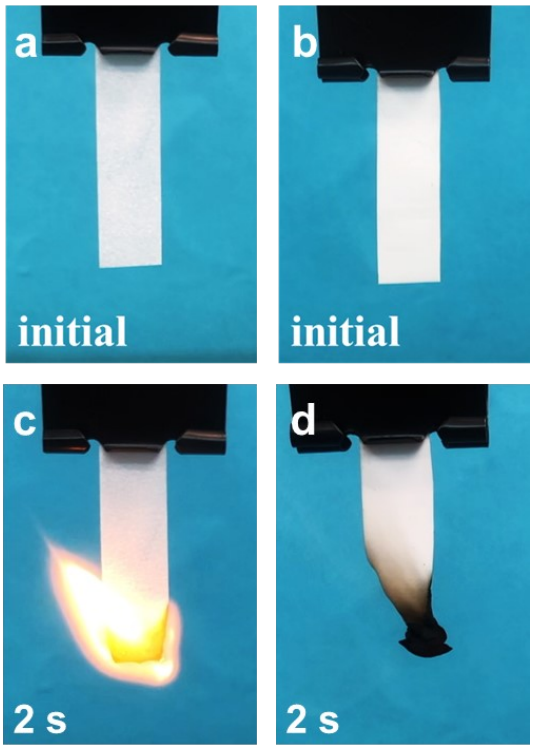

Figure S10. Pictures of the flame test on a, c) the pure PVHF-based SPE and b, d) the SPE with MIMTFSI-10-based plasticizers.

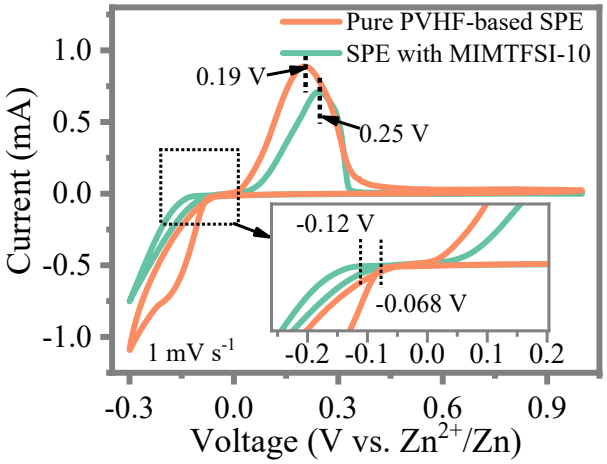

Figure S11. CV curves of the Zn‖Ti cell based on the pure PVHF-based SPE and the MIMTFSI-10-based SPE at a scan rate of 1 mV s^{-1}.

Figure S12. Optical pictures of the coin cells with the aqueous electrolyte, IL electrolyte, and SPE after cycling at 90 °C. The cells with the aqueous and IL electrolyte display evident expansion and damage, whereas the cell with the SPE shows remarkable stability, remaining unchanged throughout the cycling process.

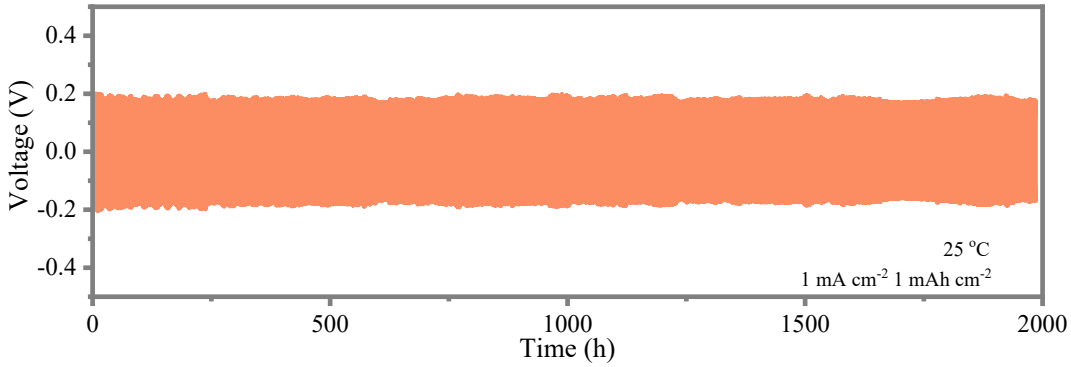

Figure S13. Cycling performance of the Zn‖Zn cell with the MIMTFSI-10-based SPE.

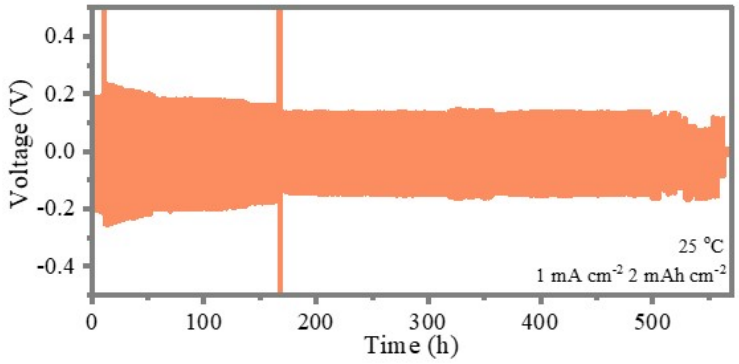

Figure S14. Cycling performance of the Zn‖Zn cell with the MIMTFSI-10-based SPE. Zinc foil with 0.01 mm thickness was employed as the anode. There is a sudden voltage increase in the cycling process of Zn‖Zn cell, which may be attributed to the external thermal instability arising as temperature changes during cycling. Such external thermal instability impacts reaction kinetics and electrolyte conductivity, leading to variations in voltage.

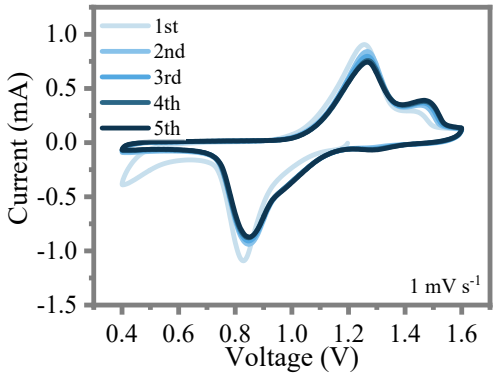

Figure S15. CV curves of the solid Zn‖Cl4Q battery at different cycles, scanned with a rate of 1 mV s^{-1}.

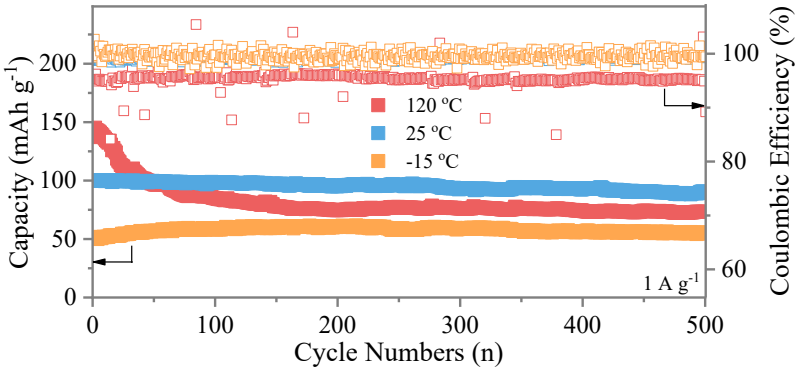

Figure S16. Long-term cycling performance of the solid Zn‖Cl4Q battery at -15 °C, 25 °C and 120 °C.

Table 1. Comparison of performance of different SPEs.

Electrolytes systems	**Ionic conductivity (mS cm^{-1})**	**t_{Zn}^{2+}**	**Polarization potential (mV, 25 °C)**	**Cycling life (h) based on Zn‖Zn cell**	**Depth of discharge (DOD, %)**	**Ref**
PVA-inter-$PEG_{30\%}/IL_{70\%}$	2.26	/	50 (0.2 mA cm^{-2})	3000 (0.2 mA cm^{-2})	0.4	6
Hbimcp/PPO	0.05	/	120 (0.1 mA cm^{-2})	200 (0.1 mA cm^{-2})	0.03	7
Poly(1,3-dioxolane)	19.6	0.7	148 (1 mA cm^{-2})	1800 (1 mA cm^{-2})	/	8
Mesoporous $Zn_yS_{1-x}F_x$	0.66	0.76	18 (5 mA cm^{-2})	1600 (5 mA cm^{-2})	41.3	9
Modified MOF-808	0.21	0.93	90 (0.1 mA cm^{-2})	360 (0.1 mA cm^{-2})	/	10
Polyzwitterionic electrolyte	32.0	0.65	220 (0.5 mA cm^{-2})	3500 (0.5 mA cm^{-2})	/	11
$PANPAN_{30\%}/Salt_{70}$	1.6	0.78	100 (0.5 mA	700 (2	3.4	12

%			cm^{-2})	mA cm^{-2})		
ZES/nano-TiO_2	0.038	0.64	20 (0.01 mA cm^{-2})	4000 (0.01 mA cm^{-2})	/	[13]
Cross-linked PAAS/LMS/CNF	0.011	0.89	60 (0.5 mA cm^{-2})	4400 (0.5 mA cm^{-2})	85.6	[14]
$ZnPS_3$	2.0	0.78	55 (0.1 mA cm^{-2})	400 (0.1 mA cm^{-2})	/	[15]
F-ILs/PVHF	2.8	0.46	195 (1 mA cm^{-2})	2000 (1 mA cm^{-2})	34.2	This work

Note: PVA: polyvinyl alcohol, PEG: polyethylene glycol, Hbimcp: 2,6-bis((propylimino)methyl)-4-chlorophenol, PPO: poly(propylene oxide), MOF-808: $[Zr_6O_4(OH)_4(HCOO)_6(BTC)_2]$, PAM: polyacrylamide, ZES: Zn^{2+} conducting solid-state electrolytes, PAAS: sodium polyacrylate, LMS: lithium magnesium silicate, CNF: cellulose nanofiber, PVHF: poly(vinylidene fluoride-co-hexafluoropropylene).

Table 2 Comparison of the electrochemical performance of different batteries at high temperatures.

Electrolyte Systems	**Working temperature (^oC)**	**Capacity (mAh g^{-1})**	**Cycling (capacity retention @ cycles)**	**Ref**
IL-AE	60	148 (1 A g^{-1})	85% @ 400	[16]
2 M $ZnSO_4$	50	410 (0.5 A g^{-1})	86% @ 50	[17]
3 M $Zn(CF_3SO_3)_2$ in PAM	60	484 (2 A g^{-1})	100% @ 100	[18]

2 M $ZnSO_4$	50	377 (5 A g^{-1})	78% @ 200	[19]
3 M $Zn(CF_3SO_3)_2$	50	378 (0.2 A g^{-1})	126% @ 50	[20]
CT3G30 gel electrolyte	60	221 (3 A g^{-1})	94% @ 2000	[21]
PAAm/DMSO/$Zn(CF_3SO_3)_2$	60	198 (10 A g^{-1})	/	[22]
F-ILs/PVHF	90	131 (1 A g^{-1})	71% @ 2000	This work

Note: IL-AE: ionic liquid-incorporated aqueous electrolyte; DMSO: dimethyl sulfoxide; PAAm: polyacrylamide; PAM: polyacrylamide.

References

1. D. Rauber, F. Heib, M. Schmitt and R. Hempelmann, *J. Mol. Liq.*, 2016, **216**, 246-258.
2. S. Grimme, J. Antony, S. Ehrlich and H. Krieg, *The Journal of Chemical Physics*, 2010, **132**, 154104.
3. D. A. Case, H. M. Aktulga, K. Belfon, I. Ben-Shalom, S. R. Brozell, D. S. Cerutti, T. E. Cheatham III, V. W. D. Cruzeiro, T. A. Darden and R. E. Duke, *Amber 2021*, University of California, San Francisco, 2021.
4. C. I. Bayly, P. Cieplak, W. Cornell and P. A. Kollman, *The Journal of Physical Chemistry*, 1993, **97**, 10269-10280.
5. E. C. Barnes, G. A. Petersson, J. A. Montgomery Jr, M. J. Frisch and J. M. Martin, *J. Chem. Theory Comput.*, 2009, **5**, 2687-2693.
6. R. Puttaswamy, Z. Tian, H. Lee, D. Y. Kim, A. Le Mong and D. Kim, *J. Mater. Chem. A*, 2023, **11**, 14075-14085.
7. D. Liu, Z. Tang, L. Luo, W. Yang, Y. Liu, Z. Shen and X.-H. Fan, *ACS Appl. Mater. Interfaces*, 2021, **13**, 36320-36329.
8. L. Ma, S. Chen, X. Li, A. Chen, B. Dong and C. Zhi, *Angew. Chem. Int. Ed.*, 2020, **59**, 23836-23844.
9. J. Zhi, S. Zhao, M. Zhou, R. Wang and F. Huang, *Sci. Adv.*, 2023, **9**, eade2217.
10. Z. Wang, J. Hu, L. Han, Z. Wang, H. Wang, Q. Zhao, J. Liu and F. Pan, *Nano Energy*, 2019, **56**, 92-99.
11. K. Leng, G. Li, J. Guo, X. Zhang, A. Wang, X. Liu and J. Luo, *Adv. Funct. Mater.*, 2020, **30**, 2001317.
12. K. Yan, Y. Fan, F. Hu, G. Li, X. Yang, X. Wang, X. Li, C. Peng, W. Wang, H. Fan and L. Ma,

Adv. Funct. Mater., 2024, **34**, 2307740.

13. H. Qiu, R. Hu, X. Du, Z. Chen, J. Zhao, G. Lu, M. Jiang, Q. Kong, Y. Yan, J. Du, X. Zhou and G. Cui, *Angew. Chem. Int. Ed.*, 2022, **61**, e202113086.
14. C. Yang, P. Woottapanit, S. Geng, R. Chanajaree, Y. Shen, K. Lolupiman, W. Limphirat, T. Pakornchote, T. Bovornratanaraks, X. Zhang, J. Qin and Y. Huang, *Nat. Commun.*, 2025, **16**, 183.
15. Z. Lv, Y. Kang, G. Chen, J. Yang, M. Chen, P. Lin, Q. Wu, M. Zhang, J. Zhao and Y. Yang, *Adv. Funct. Mater.*, 2024, **34**, 2310476.
16. L. Yu, J. Huang, S. Wang, L. Qi, S. Wang and C. Chen, *Adv. Mater.*, 2023, **35**, 2210789.
17. Y. Yang, Y. Tang, S. Liang, Z. Wu, G. Fang, X. Cao, C. Wang, T. Lin, A. Pan and J. Zhou, *Nano Energy*, 2019, **61**, 617-625.
18. W. Deng, Z. Zhou, Y. Li, M. Zhang, X. Yuan, J. Hu, Z. Li, C. Li and R. Li, *ACS Nano*, 2020, **14**, 15776-15785.
19. B. Tang, J. Zhou, G. Fang, F. Liu, C. Zhu, C. Wang, A. Pan and S. Liang, *J. Mater. Chem. A*, 2019, **7**, 940-945.
20. N. Zhang, Y. Dong, M. Jia, X. Bian, Y. Wang, M. Qiu, J. Xu, Y. Liu, L. Jiao and F. Cheng, *ACS Energy Lett.*, 2018, **3**, 1366-1372.
21. M. Chen, J. Chen, W. Zhou, X. Han, Y. Yao and C.-P. Wong, *Adv. Mater.*, 2021, **33**, 2007559.
22. H. Lu, J. Hu, L. Wang, J. Li, X. Ma, Z. Zhu, H. Li, Y. Zhao, Y. Li, J. Zhao and B. Xu, *Adv. Funct. Mater.*, 2022, **32**, 2112540.